

The relativistic jet of Cygnus X-3 in gamma rays

G. Dubus, B. Cerutti and G. Henri

Laboratoire d'Astrophysique de Grenoble, UMR 5571 Université Joseph Fourier Grenoble I / CNRS, BP 53, 38041 Grenoble, France

Accepted . Received ; in original form 18 November 2018

ABSTRACT

High energy gamma-rays have been detected from Cyg X-3, a system composed of a Wolf-Rayet star and a black hole or neutron star. The gamma-ray emission is linked to the radio emission from the jet launched in the system. The flux is modulated with the 4.8 hr orbital period, as expected if high energy electrons are upscattering photons emitted by the Wolf-Rayet star to gamma-ray energies. This modulation is computed assuming that high energy electrons are located at some distance along a relativistic jet of arbitrary orientation. Modelling shows that the jet must be inclined and that the gamma ray emitting electrons cannot be located within the system. This is consistent with the idea that the electrons gain energy where the jet is recollimated by the stellar wind pressure and forms a shock. Jet precession should strongly affect the gamma-ray modulation shape at different epochs. The power in non-thermal electrons represents a small fraction of the Eddington luminosity only if the inclination is low *i.e.* if the compact object is a black hole.

Key words: radiation mechanisms: non-thermal — stars: individual (Cygnus X-3) — ISM: jets and outflows — gamma rays: theory — X-rays: binaries

1 INTRODUCTION

Cyg X-3 is a high-mass X-ray binary composed of a compact object in a 4.8 hr orbit around a Wolf-Rayet (WR) star at a distance of about 7 kpc (see Bonnet-Bidaud & Chardin 1988; van Kerkwijk et al. 1996; Ling et al. 2009, and references therein). The system is a bright X-ray source with $L_X \approx 10^{38}$ erg s $^{-1}$. Cyg X-3 is also well-known for radio flaring (up to 20 Jy) when the source has a soft X-ray spectra (Szostek et al. 2008). The radio source is resolved into a relativistic jet with an expansion speed of 0.3-0.7c. The strong stellar wind from the WR companion ($\dot{M}_w \approx 10^{-5} M_\odot \text{yr}^{-1}$, $v_w \approx 1000$ km s $^{-1}$) has a major impact on the environment of the high-energy source. Scattering in the wind is probably responsible for washing out rapid X-ray variability timescales and also for modulating the X-ray emission. It acts as a veil that has made it difficult to identify the nature of the compact object, black hole or neutron star. Despite the differences caused by the WR wind, Cyg X-3 is firmly established as a trademark accreting binary with relativistic jet *i.e.* a microquasar.

The *AGILE* and the *Fermi Gamma-ray Space Telescope* collaborations have recently reported the detection of high-energy gamma rays (HE, >100 MeV) from Cyg X-3 (Tavani et al. 2009; Abdo et al. 2009). The identification is firm because the detections occur exclusively when Cyg X-3 is flaring in radio and because *Fermi* observations show the HE gamma-ray flux is modulated with the orbital period. The gamma-ray modulation is almost in anti-phase with

the X-ray modulation, with the gamma-ray minimum occurring about 0.3-0.4 in phase after X-ray minimum. The modulation amplitude is close to 100% after background subtraction. The spectrum is consistent with a power law $F_\nu \sim \nu^{-\alpha}$ with $\alpha = 1.7$. The luminosity above 100 MeV is a few $10^{36} (d/7 \text{ kpc})^2$ erg s $^{-1}$.

Inverse Compton (IC) scattering of photons from the WR star on high energy electrons is a natural candidate to explain the gamma-ray emission. The high temperature of the WR star ($R_\star \approx 1 R_\odot$, $T_\star \approx 10^5$ K) and tight orbit ($d \approx 3 \cdot 10^{11}$ cm) imply that the radiation density in photons from the star is $u_\star \approx 10^5$ erg cm $^{-3}$ at the location of the compact object, which is at least an order-of-magnitude higher than any other X-ray binary. Electrons with Lorentz factors of a few 10^3 upscatter 20 eV stellar photons above 100 MeV very efficiently in such a radiation field. IC scattering directly produces a modulation of the flux because of the orbital motion. The maximum occurs when stellar photons are backscattered towards the observer. The accretion disc can also provide seed photons if the HE electrons are close enough. This does not lead to a modulation unless the HE electrons - disk geometry seen by the observer changes with orbital phase (Meszaros et al. 1977). Pion production is possible if there are high energy protons. However, even in this dense environment, it is less efficient than IC so that its energy requirements are higher.

The link between gamma-ray and radio flares suggests that the HE electrons are located in the relativistic jet. Observations of knots in active galactic nuclei show that

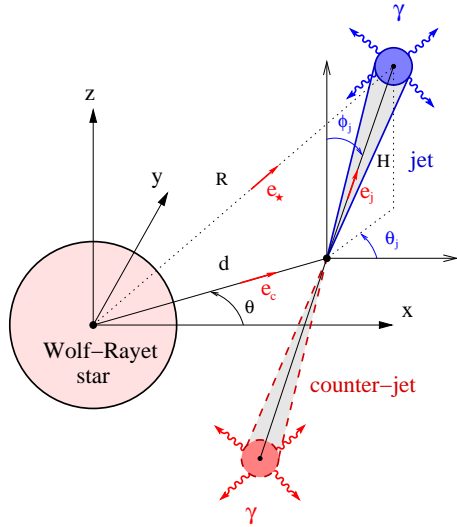


Figure 1. Geometry of the jet model. The scattering electrons are situated at symmetric locations in a jet with relativistic speed β . The seed photon source is the star.

particles may be accelerated at specific locations along the jet, linked *e.g.* to recollimation shocks (Stawarz et al. 2006). Assuming the electrons mainly upscatter stellar photons at some location along the jet, the expected IC emission will depend upon the distance to the star, the bulk velocity of the jet and its orientation. This orientation is not necessarily perpendicular to the orbital plane *e.g.* the inner accretion disc is warped or it depends on the black hole spin axis. However, the jet orientation is fixed as seen by the observer (changing only if the jet precesses).

The goal here is to test quantitatively whether the *Fermi* gamma-ray modulation can be reproduced in this framework and to see if constraints can be derived on the jet parameters.

2 JET INVERSE COMPTON EMISSION

2.1 Emission spectrum

The HE electrons are assumed to be located at a distance H from the compact object along a jet with a bulk velocity $\beta = v/c$ (Fig. 1). The stellar emission is approximated as a point-like blackbody of temperature T_* and luminosity $4\pi R_*^2 \sigma_{SB} T_*^4$. The electron Lorentz factors γ_e are distributed as a power-law $dN_e = K_e \gamma_e^{-p} d\gamma_e$. In the Thompson regime, the inverse Compton emission spectrum at a photon energy ϵ (in ergs) is given by (Dubus et al. 2010)

$$F_{IC} \equiv \epsilon \frac{dN}{dt d\epsilon} = \frac{C(p) K_e \pi \left(\frac{R}{R_*}\right)^2 (kT_*)^{\alpha+3}}{\times \mathcal{D}_{\text{obs}}^{4+2\alpha} (1 - \mathbf{e}_* \cdot \mathbf{e}_{\text{obs}})^{\alpha+1} \epsilon^{-\alpha}} \quad (1)$$

where: the flux index is related to the electron power law index through $\alpha = (p-1)/2$, R is the distance from the star to the electron location; \mathbf{e}_* and \mathbf{e}_{obs} are unit vectors along, respectively, the star-to-electrons and the electrons-to-observer directions;

$$\mathcal{D}_{\text{obs}} = \frac{(1 - \beta^2)^{1/2}}{(1 - \beta \mathbf{e}_{\text{obs}} \cdot \mathbf{e}_{\text{jet}})} \quad (2)$$

defined the Doppler boost of the jet, \mathbf{e}_{jet} being the unit vector along the jet direction; $C(p)$ is given by

$$C(p) = \frac{\pi r_e^2 c^2 2^{\frac{p+5}{2}} (p^2 + 4p + 11) \Gamma\left(\frac{p+5}{2}\right) \zeta\left(\frac{p+5}{2}\right)}{h^3 c^3 (p+1)(p+3)(p+5)} \quad (3)$$

with Γ the gamma function and ζ the Riemann function. This formula is valid in the Thompson regime, that is when $\gamma_e \epsilon_0 < m_e c^2$ where ϵ_0 is the characteristic energy of the seed photons. For a blackbody with $T_* = 10^5$ as in Cyg X-3, $\epsilon_0 \approx 2.7 kT_* \approx 23$ eV so the limit occurs for $\gamma_e \approx 2 \cdot 10^4$ (neglecting the Doppler boost). IC emission from 100 MeV to a few GeV (the relevant *Fermi* range) occurs in the Thompson regime.

The model geometry is shown in Fig. 1. The jet has an azimuth θ_j and polar angle ϕ_j ($=0$ when perpendicular to orbital plane). With the origin set at the location of the WR star,

$$R^2 = d^2 + H^2 + 2dH(\mathbf{e}_c \cdot \mathbf{e}_{\text{jet}}) \quad (4)$$

where \mathbf{e}_c is the unit vector along the star to compact object direction, and the unit vectors are given by

$$\begin{aligned} \mathbf{e}_* &= (d\mathbf{e}_c + H\mathbf{e}_{\text{jet}})/R \\ \mathbf{e}_{\text{jet}} &= (\cos \theta_j \sin \phi_j, \sin \theta_j \sin \phi_j, \cos \phi_j) \\ \mathbf{e}_c &= (\cos \theta, \sin \theta, 0) \\ \mathbf{e}_{\text{obs}} &= (0, -\sin i, \cos i) \end{aligned} \quad (5)$$

with θ the true anomaly, d the orbital separation and i the inclination. Here, the true anomaly is defined so that $\theta = \pm\pi/2$ at conjunctions.

2.2 Main properties

The inverse Compton emission has an orbital modulation because of the dependence of \mathbf{e}_c on the true anomaly ($=$ orbital phase for a circular orbit). Developing $\partial F_{IC}/\partial \theta = 0$, the emission maximum and minimum along the orbit verify:

$$(\alpha+1)(\mathbf{e}_c \times \mathbf{e}_{\text{obs}}) \cdot \mathbf{e}_z = \frac{H}{R} ((\alpha+3)\mathbf{e}_* \cdot \mathbf{e}_{\text{obs}} - 2)(\mathbf{e}_c \times \mathbf{e}_{\text{jet}}) \cdot \mathbf{e}_z \quad (6)$$

If $H \ll d$, or if the jet is perpendicular to the orbital plane, then the maxima and minima are at conjunctions as outlined in §1. Otherwise, they occur at orbital phases that can be very different.

The IC flux will be equal to zero if $\mathbf{e}_* \cdot \mathbf{e}_{\text{obs}} = 1$ somewhere along the orbit. Having a 100% modulation can be translated into a necessary condition on H for given i , d , ϕ_j and θ_j . Similarly, although the seed photon density decreases with H , the maximum of the IC flux for a given jet geometry does not necessarily occur for $H=0$ because of the dependence of \mathbf{e}_* on H .

The jet speed only appears in \mathcal{D}_{obs} and $\mathbf{e}_{\text{obs}} \cdot \mathbf{e}_{\text{jet}}$ is constant along the orbit: changing β will only impact the flux normalisation and not the shape of the modulation. The maximum flux occurs when $\beta = \mathbf{e}_{\text{obs}} \cdot \mathbf{e}_{\text{jet}}$. Emission from a jet oriented away from the observer will always be weak for highly relativistic speeds because of the deboost.

3 APPLICATION TO CYG X-3

The observed modulation is plotted in Figure 2. The background level in diffuse gamma rays of $3.6 \cdot 10^{-6}$ ph cm $^{-2}$ s $^{-1}$ was subtracted to the *Fermi* lightcurve (Abdo et al.

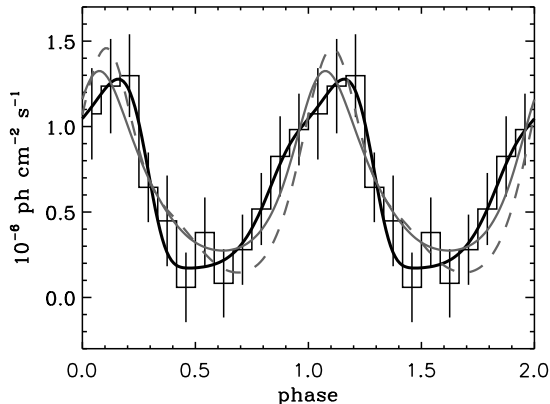


Figure 2. Model fits to the observed > 100 MeV gamma-ray modulation in Cyg X-3. Conjunctions are at phases 0.25 and 0.75 for the conventions adopted in this work. The models shown assumed an orbit with a black hole (O1). The best model is shown with a black solid line. A model with $\beta = 0$ is shown with a grey solid line. The model with minimum P_e ($3 \cdot 10^{33} \text{ erg s}^{-1}$) is shown with a grey dashed lines. All of these models are statistically acceptable fits to the data (see §3 for details).

2009). There is not absolute phasing of the orbit of Cyg X-3. The *Fermi* observations have been phased so that the well-defined minimum X-ray flux occurs at superior conjunction i.e. phase 0.25 with the conventions adopted in this paper (Fig. 1). This phasing is justified if the X-ray modulation is due to Thompson scattering in the stellar wind (Pringle 1974). It is independently supported by infrared spectroscopy (Hanson et al. 2000).

The orbital parameters of Cyg X-3 are not determined precisely (Hanson et al. 2000; Vilhu et al. 2009) so two extreme solutions are adopted following Szostek & Zdziarski (2008). Orbit 1 (O1) has a $M_1=20 M_\odot$ black hole around a $50 M_\odot$ WR star of radius $2.3 R_\odot$ and is seen with an inclination of 30° . Orbit 2 (O2) has a $M_1=1.4 M_\odot$ neutron star around a $5 M_\odot$ WR star of radius $0.6 R_\odot$ with $i = 70^\circ$. The *Fermi* spectrum $\alpha = 1.7$ sets the electron power-law index $p = 4.4$. The emission arise from two symmetric sites: the jet and the counterjet. The counterjet has $\phi_{c,j} = \pi + \phi_j$.

3.1 Parameter exploration

The jet is parametrised by β , H , ϕ_j , θ_j and K_e . The expected modulation in the *Fermi* band is calculated using the equation in §2 for the jet and the counterjet. The evaluation of Eq. 1 is very fast and allows an exhaustive exploration of the parameter space. The jet angle ϕ_j was varied between 0 and $\pi/2$; θ_j varied between 0 and 2π . The emission height H was varied between $0.01d$ and $100d$ in logarithmic steps (d is the orbital separation). The jet speed β was varied linearly from 0 to 0.99 (bulk Lorentz factor ≈ 7).

The model K_e is adjusted to minimize the χ^2 goodness-of-fit to the observed modulation. The normalisation K_e is converted into a power in HE electrons P_e assuming a distance of 7 kpc and a minimum HE electron Lorentz factor $\gamma_{e,\min} = 1000$. P_e is highly sensitive to $\gamma_{e,\min}$ because of the very steep electron spectrum. IC emission above 100 MeV

requires that $\gamma_{e,\min} \leq 1000$ so P_e is a lower limit on the non-thermal power.

Good fits can be obtained for both O1 ($\chi_{\min}^2 = 2.7$ for 12 data points - 5 parameters = 7 degrees of freedom) and O2 ($\chi_{\min}^2 = 4.2$). The best model for O1 is plotted in Figure 2. It has $\beta = 0.41$, $H = 8 \cdot 10^{11} \text{ cm}$, $\phi_j = 39^\circ$, $\theta_j = 319^\circ$, $P_e = 10^{38} \text{ erg s}^{-1}$. The 90% confidence range for the parameters was determined by adding 9.24 to the minimum χ^2 (Lampton et al. 1976). Only models that had P_e lower than the Eddington luminosity $L_{\text{Edd}} \approx 10^{38} (M_1/M_\odot) \text{ erg s}^{-1}$ were kept. Besides being physically implausible, models with larger P_e are associated with high values of β or large H . The high P_e then compensates for Doppler deboosting or low IC efficiency (see §3.3).

3.2 Jet orientation

Figure 3 shows the distributions of β , H , ϕ_j and θ_j for the black hole case (O1). The figure also shows the distributions for various limits on P_e . In all cases, the HE electrons distance H is between 0.5 and 30 times the orbital separation (i.e. between $2 \cdot 10^{11}$ and 10^{13} cm). A location very close to the compact object is excluded. The orientation of the jet is constrained to be $20^\circ \lesssim \phi_j \lesssim 80^\circ$ with a preference for values comparable to the system inclination ($i = 30^\circ$). A jet perpendicular to the orbital plane does not fit the data. The azimuth θ_j is less constrained: there is a well defined peak in the distribution (bottom panel, Fig. 3) but, contrary to H or ϕ_j , there are good models all over the range even in small numbers (not visible on a linear scale).

Moderate relativistic speeds β are favoured but this is not strongly constrained. The speed is closely linked to the power in HE electrons. There is a tendency to have lower values of β when the allowed P_e gets smaller, accompanied by a smaller H . A model in the 90% confidence region with $\beta=0$ is shown in Figure 2. It has $\chi^2 = 7.1$, $H = 7 \cdot 10^{11} \text{ cm}$, $\phi_j = 31^\circ$, $\theta_j = 9^\circ$, $P_e = 2 \cdot 10^{37} \text{ erg s}^{-1}$. This trend on β reverses for low values of $P_e \lesssim 0.001 L_{\text{Edd}}$. These do not appear in Figure 3 as there are comparatively very few such models. The minimum P_e in the 90% confidence region is $4 \cdot 10^{33} \text{ erg s}^{-1}$, a very modest fraction of L_{Edd} . This model is also shown in Figure 2. It has $\chi^2 = 11.3$, $\beta = 0.99$, $H = 10^{12} \text{ cm}$, $\phi_j = 32^\circ$ and $\theta_j = 275^\circ$. These low P_e models all have $\phi_j \approx i$ and $\theta_j \approx -90^\circ$: they are almost aligned with the observer ($\mathbf{e}_{\text{jet}} \cdot \mathbf{e}_{\text{obs}} \approx 1$) at superior conjunction. The slight difference in θ_j accounts for the phase difference of the maximum. Here, Doppler boosting compensates for the low P_e . There is some degeneracy between the two parameters up to some (large) value of the Lorentz factor ≈ 20 where good models cannot be found anymore. These are effectively microblazar models.

The constraints in the neutron star case (orbit O2, not shown here) are similar. The jet orientation is well constrained with $25^\circ \lesssim \phi_j \lesssim 65^\circ$, $-60^\circ \lesssim \theta_j \lesssim -10^\circ$ and $2 \cdot 10^{11} \text{ cm} \lesssim H \lesssim 6 \cdot 10^{11} \text{ cm}$ (H/d from 1 to 3), comparable to the values found with O1. However, in all cases β is $\lesssim 0.2$. Interestingly, P_e is constrained to be rather large with $P_e \gtrsim 0.2 L_{\text{Edd}}$ (about $3 \cdot 10^{37} \text{ erg s}^{-1}$). The large inclination (70°) required for a neutron star primary is the reason for the difference with the black hole case. Arbitrarily setting $i = 30^\circ$ with the orbit O2 gives results for β and P_e that are

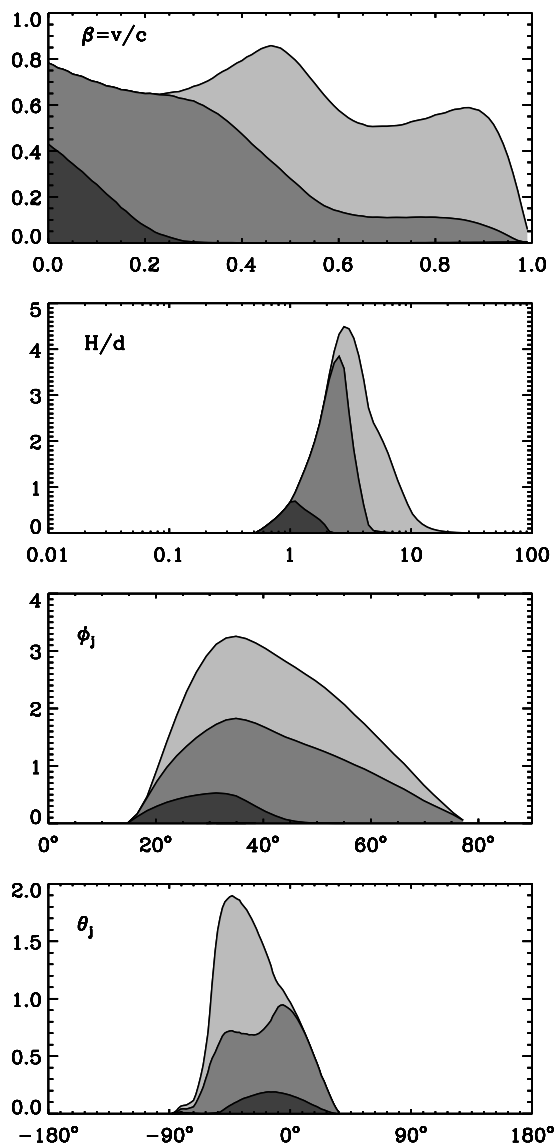


Figure 3. Distribution of jet parameters for models in the 90% confidence region given by χ^2 statistics. Orbit O1 (20 M_{\odot} black hole, $i=30^\circ$) is assumed. The various regions correspond to a power in high energy electrons $P_e \leq L_{\text{Edd}}$ (light grey), $\leq 0.1L_{\text{Edd}}$ (grey), $\leq 0.01L_{\text{Edd}}$ (dark grey). Here, L_{Edd} is $2 \cdot 10^{39}$ erg s^{-1} .

consistent with those of O1. Large inclinations do not allow good fits for small values of P_e or large values of β .

These results were obtained for a steep power-law distribution of electrons with an index $p = 4.4$, because of the soft gamma-ray flux index and the assumption of Thompson scattering. Taking $p = 2$ or $p = 3$ does not affect the conclusions. A few test calculations using the full IC cross section (done as explained in Dubus et al. 2010) showed that a slightly harder electron index ($p \approx 4$) is required to match the spectrum. Again, this does not change the results. The steep spectrum may not directly reflect an electron power-law distribution but represent the best fit to *e.g.* a cutoff in the 100 MeV – 1 GeV range. To test this, a lightcurve

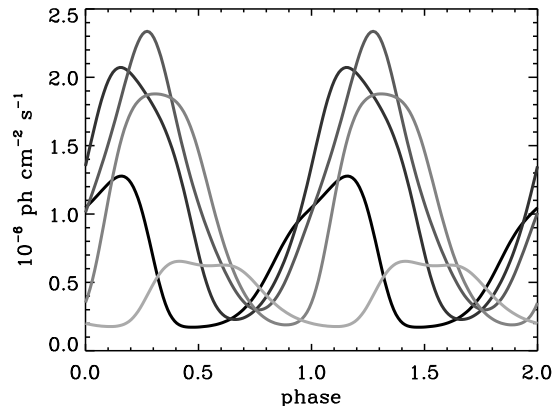


Figure 4. Impact of jet precession on the gamma-ray lightcurve for the best-fit model shown in Figure 2. The jet azimuth θ_j is rotated in steps of 72° from its best fit value of 319° , with lighter lines as θ_j moves away from this value.

was calculated (including the full IC cross section) for a jet with the parameters of the best fit shown in Fig. 2 but assuming a power law distribution $p = 3$ from $\gamma_e = 100$ up to $\gamma_{e,\text{cutoff}} \approx 3 \cdot 10^3$. (A $p = 3$ slope is expected for a steady state distribution of electrons injected with the canonical $p = 2$ power law in the presence of strong Thompson IC cooling.) The >100 MeV lightcurve was indistinguishable from the one in Fig. 2, even though the cutoff energy changed significantly along the orbit due to Doppler boosting. Hence, the results obtained here are likely to extend when more complex spectral shapes and Klein-Nishina effects are taken into account.

3.3 Jet precession

The preceding section showed that the jet must be inclined in order to obtain good fits to the gamma-ray modulation. There is evidence for jet inclination in Cyg X-3 as well as other microquasars (Maccarone 2002). An inclined jet is likely to undergo precession on a timescale longer than the orbital period. There is currently no evidence for or against jet precession in Cyg X-3. Here, jet precession will manifest itself as a change in the gamma-ray modulation since θ_j will sample the full range from 0 to 2π in a full precession. Both the shape and amplitude are affected as shown in Figure 4. The peak flux phase and amplitude can vary dramatically from one precession phase to another.

The *Fermi* data already show a hint for a change in the phasing of the modulation between the two epochs during which Cyg X-3 was detected. In addition, the first reported detection of Cyg X-3 at 100 MeV from SAS-2 showed a gamma-ray orbital modulation correlated (instead of roughly anti-correlated) with the X-ray modulation (Lamb et al. 1977). Later observations by *Cos B* and EGRET failed to re-detect the source unambiguously (Mori et al. 1997). A possible explanation is that the jet orientation had changed in between these observations. Future *Fermi* observations of Cyg X-3 may find a different modulation lightcurve or may actually fail to detect the source

because of its low flux, even though Cyg X-3 shows the right radio and X-ray state.

The comparison between gamma-ray lightcurves can serve as a very powerful diagnostic of the jet geometry. For instance, in the microblazar models discussed in §3.2, the near perfect alignment of a jet with the line-of-sight and the high β means that the gamma-ray flux is detectable only during the very short interval in precession phase where it is Doppler boosted. The gamma-ray flux will be deboosted most of the time — so that the *Fermi* and *AGILE* detections would have required very special circumstances.

4 CONCLUSIONS

The orbital modulation of the >100 MeV flux from Cyg X-3 can be very well fitted by a simple-minded model in which the emission is due to HE electrons up-scattering stellar photons. The HE electrons are situated in two symmetric locations in a relativistic jet with an arbitrary orientation.

The fitting procedure reveals that the jet is necessarily inclined to the orbital plane normal. The most likely value is close to the line-of-sight ($\phi_j \approx i$, in agreement with the conclusions based on radio imaging of the jet (Mioduszewski et al. 2001). The HE electrons cannot be close to the compact object. They are outside of the system at distances of at least one orbital separation, possibly up to $10d$. IC scattering of accretion disc photons is then irrelevant. If the compact object in Cyg X-3 is a neutron star, the required power in HE electrons is a significant fraction of the Eddington luminosity. For a black hole, because of the lower system inclination implied, the power required can be as low as $10^{-5} L_{\text{Edd}}$. These conclusions appear robust even when more complex electron distributions and the full IC cross-section are taken into account. Precession can be expected from an inclined jet. It should cause a change in the shape and amplitude of the gamma-ray modulation in the future.

The IC cooling timescale is $t_{\text{ic}} \approx 0.5(\gamma_e/10^3)^{-1}(R/d)^2$ seconds (scaled to the orbital separation d and for orbit O1). The size of the gamma ray emitting region is roughly $s \approx \beta c t_{\text{ic}}$, giving $s/R \lesssim 0.04\beta(\gamma_e/10^3)^{-1}(R/d)$ when scaled to R . Hence, the assumption that the emission in the *Fermi* energy range is localised holds up to distances $\approx 10d$ from the star. Cooling slows down at lower energies and electrons emit synchrotron radio beyond the γ -ray emission zone on much larger scales.

The γ -ray emission zone could be related to electron acceleration at a recollimation shock as the jet pushes its way through the stellar wind. The jet is initially over-pressured compared to its environment. It expands freely until its pressure p_j matches that of the environment p_e . Here, p_e is the ram pressure of the supersonic wind $\rho_w v_w^2$. The jet pressure is $p_j \sim L_j/(\pi c \Theta^2 l^2)$ where L_j is the jet power, Θ is its opening angle and l is the distance along the jet (e.g. Bednarek & Protheroe 1997). The pressures equilibrate at

$$\frac{l}{R} \sim 0.5 \Theta^{-1} L_{38}^{1/2} \dot{M}_{-5}^{-1/2} v_{1000}^{-1/2} \quad (7)$$

with $L_j = 10^{38}$ erg s $^{-1}$, $\dot{M}_w = 10^{-5} M_{\odot}$ yr $^{-1}$ and $v_w = 1000$ km s $^{-1}$. A jet recollimation shock forms beyond l . The shock crosses the jet axis after a further distance of order l

when the external pressure is constant (Stawarz et al. 2006). This is roughly the case here since the jet does not extend very far from the system and the dependence of p_w with l remain shallow (unless it is pointed directly away from the star). The location is consistent with the values of H derived above, suggesting this is where jet kinetic or magnetic energy is channeled into particle acceleration. This should be verified by calculations taking into account the non-radial nature of the jet-wind interaction. The shock occurs in the wind only because \dot{M}_w is very large (WR star) and the orbit very tight. Most microquasar jets will actually break out of the immediate vicinity of the system and interact much further away when their pressure matches that of the ISM. Any HE particles there will find a much weaker radiation environment and will be less likely to produce a (modulated) IC gamma-ray flux detectable by *Fermi* or *AGILE*.

The emerging picture is that of a jet launched around a black hole, with a moderate bulk relativistic speed, oriented not too far from the line-of-sight, interacting with the WR stellar wind to produce a shock at a distance of $1-10d$ from the system, where electrons are accelerated to GeV energies and upscatter star photons.

ACKNOWLEDGMENTS

The authors thank S. Corbel, J.-P. Lasota, L. Stawarz and A. Szostek for comments. This work was supported by the European Community via contract ERC-StG-200911.

REFERENCES

- Abdo A. A., et al. (*Fermi*-LAT collaboration) 2009, *Science*, 326, 1512
- Bednarek W., Protheroe R. J., 1997, *MNRAS*, 287, L9
- Bonnet-Bidaud J. M., Chardin G., 1988, *Phys. Rep.*, 170, 326
- Dubus G., Cerutti B., Henri G., 2010, *A&A*, submitted
- Hanson M. M., Still M. D., Fender R. P., 2000, *ApJ*, 541, 308
- Lamb R. C., Fichtel C. E., Hartman R. C., Kniffen D. A., Thompson D. J., 1977, *ApJ*, 212, L63
- Lampton M., Margon B., Bowyer S., 1976, *ApJ*, 208, 177
- Ling Z., Zhang S. N., Tang S., 2009, *ApJ*, 695, 1111
- Maccarone T. J., 2002, *MNRAS*, 336, 1371
- Meszaros P., Meyer F., Pringle J. E., 1977, *Nature*, 268, 420
- Mioduszewski A. J., Rupen M. P., Hjellming R. M., Pooley G. G., Waltman E. B., 2001, *ApJ*, 553, 766
- Mori M., et al. 1997, *ApJ*, 476, 842
- Pringle J. E., 1974, *Nature*, 247, 21
- Stawarz L., Aharonian F., Kataoka J., Ostrowski M., Siemiginowska A., Sikora M., 2006, *MNRAS*, 370, 981
- Szostek A., Zdziarski A. A., 2008, *MNRAS*, 386, 593
- Szostek A., Zdziarski A. A., McCollough M. L., 2008, *MNRAS*, 388, 1001
- Tavani M., et al. (*AGILE* collaboration) 2009, *Nature*, 462, 620
- van Kerkwijk M. H., Geballe T. R., King D. L., van der Klis M., van Paradijs J., 1996, *A&A*, 314, 521

Vilhu O., Hakala P., Hannikainen D. C., McCollough M.,
Koljonen K., 2009, A&A, 501, 679